J. Fluid Mech. (2000), *vol.* 420, *pp.* 27–46. Printed in the United Kingdom

© 2000 Cambridge University Press

An analytical model of gravity currents in a stable atmosphere

By YIZHAK FELIKS

Department of Mathematics, Israel Institute of Biological Research, Ness-Ziona, 70450, Israel

(Received 26 September 1997 and in revised form 20 March 2000)

An analytical solution to the nonlinear equations of motion and thermodynamic energy for gravity currents propagating in stable atmosphere is found. This solution differs from the previous analytical studies in several aspects. In our solution the head of the gravity current is a strong vortex and the dynamics are non-hydrostatic. The solution has two regimes: (i) a supercritical regime when the Froude number $Fr = (c - U)/Na$ is larger than 1 – in this case the cold front is local; (ii) a subcritical regime when Fr is smaller than 1. Here, ahead of the front there is a disturbance of nonlinear gravity waves. The scale of the wave and its amplitude increase as the Froude number decreases.

We found that the square of the speed of the gravity current (relative to the synoptic wind) is proportional to the mean drop of potential temperature over the front area times the front height a. The constant of proportionality is function of the environmental conditions. The thermal, velocity and vorticity fields can be described by non-dimensional structure functions of two numbers: $pa = 1/Fr$ and ka. The amplitude of the structure functions is proportional to $(c - U)^2/a$ for the thermal field, to $(c - U)$ for the velocity field, and to $(c - U)/a$ for the vorticity field.

The propagation is studied in terms of the vorticity equation. The horizontal gradient of the buoyancy term always tends to propagate the cold front. The nonlinear advection term in most of the cases investigated here tends to slow the propagation of the gravity current. The propagation of the disturbance of nonlinear gravity waves ahead of the front in regime (ii) in most of the cases is due to the buoyancy term. The nonlinear advection term tends to slow the propagation when the synoptic wind blows in the direction opposite to that of the front propagation, and increase the propagation when the synoptic wind blows in the direction of propagation.

1. Introduction

Many examples of gravity currents of cold air moving into warmer air observed in the atmosphere, called cold fronts, have been observed, see for example Pearson (1973), Simpson, Mansfield & Milford (1977), Atkinson (1981), and Haase (1991). The scale of these fronts is about 1 km. In these cold fronts the Earth's rotation is negligible while the non-hydrostatic dynamics is important. In the following we shall discuss fronts of this kind and not the synoptic-scale fronts. Cold fronts moving in a neutral atmosphere have been observed and studied extensively in recent years, see for example Haase & Smith (1989*a*, *b*), Xu (1992), Xu, Xue & Droegemeier (1996) and Liu & Moncrieff (1996). Most of those model studies are numerical owing to the nonlinear nature of the problem. An analytical attempt to study different stages of the evolution of a density current can be found in Benjamin (1968). He obtained an

https://doi.org/10.1017/S0022112000001488 Published online by Cambridge University Press

expression for the speed of the gravity current which is proportional to the density jump across the front and to the front's height.

Feliks (1988) solved analytically the nonlinear equation of motion and the thermodynamic energy equation in a neutral environment for the case of a steady, propagating front. The front has a complicated flow with very strong vertical velocities of up to several metres per second. The wind in the lower part of the front has a strong convergence and there is a return current (associated with the strong divergence obtained) in the upper part of the front. Such a front resembles the sea breeze front. The horizontal gradient of the buoyancy tends to propagate the front, whereas the nonlinear advection terms in most of the cases tend to slow this propagation.

Crook & Miller (1985) and Haase & Smith (1989*b*) studied numerically the evolution of a cold front propagating into a stable environment, where above the stable layer the atmosphere stability was assumed to be neutral. They found two regimes in the solution: subcritical and supercritical. The subcritical regime is defined as when the disturbance of gravity waves (in the free atmosphere outside the front) initiated by the translation of the gravity current (cold front) propagates a considerable distance ahead of the front. This disturbance can take the form of a solitary wave, or an undular bore. The supercritical regime is defined as when the propagation speed of the disturbance is less than the speed of the gravity current. In this case the front can be considered as local.

Liu & Moncrieff (1996) studied analytically the density current propagation in stratified, sheared fluids. Their results show that stable stratification decreases the depth of the density current and increases the propagation speed. Their result differs sharply from the solution of Benjamin (1988) in which the propagation speed is proportional to the depth. In their studies they assumed that the flow in the cold front was motionless relative to the moving front. Moreover the role of gravity waves and their interaction with the gravity current to form an undular bore in a strongly stratified atmosphere and its influence on the speed of the gravity current were not included in their study. Thus their result may change significantly when those effects are included.

In the following we solved analytically the equations of inviscid motion and thermodynamic energy in a stable atmosphere, as in Feliks (1988). This solution enables us to study in detail the parameters which influence the front structure, its propagation speed, and the causes of its propagation. The solution described in this paper and that of Feliks (1988) differ from the previous analytical solutions of gravity currents in several aspects. Here the shape of the front is prescribed, and the density and velocity are determined by the solution and are continuous on the interface; only their derivative is discontinuous. In previous studies the density is prescribed, the shape of the front and the velocity are determined by the solution, and the velocity and density are discontinuous on the interface. In our solution there is intensive circulation with strong vorticity inside the gravity current and the dynamics is non-hydrostatic. Such circulation has been observed in the atmospheric gravity currents. In almost all the previous studies the flow inside the gravity current is motionless (in a relative frame of reference) so the effect of the dynamics is excluded and the hydrostatic approximation is used to determine the internal pressure on the interface. The exception is the study of Xu & Moncrieff (1994) where circulation in the gravity head was considered. Since the vorticity in their study was constant, the propagation of the head does not depend on the circulation in the head. In our solution the vorticity in the head is not constant and the propagation of the gravity current depends on the vorticity structure, as will be shown in § 5.

https://doi.org/10.1017/S0022112000001488 Published online by Cambridge University Press

2. Formulation of the problem

We deal with fronts which are limited to the lower atmosphere; hence their heights are much smaller than the scale height of the atmosphere. This allows us to use the Boussinesq incompressible approximation of the equations of motion:

$$\frac{\partial u}{\partial t} + u\frac{\partial u}{\partial x} + w\frac{\partial u}{\partial z} = -\frac{1}{\rho_m}\frac{\partial P}{\partial x}, \tag{2.1}$$

$$\frac{\partial w}{\partial t} + u\frac{\partial w}{\partial x} + w\frac{\partial w}{\partial z} = -\frac{1}{\rho_m}\frac{\partial P}{\partial z} - \frac{\rho g}{\rho_m}, \tag{2.2}$$

$$\frac{\partial u}{\partial x} + \frac{\partial w}{\partial z} = 0. \tag{2.3}$$

Here $u = u' + U$, U is the undisturbed wind speed ahead of the front and we will refer to it as the synoptic wind speed; u' and w are the perturbation velocity components, ρ_m is a mean reference density, and P and ρ are the perturbation pressure and density. For simplicity the Coriolis force and viscosity effects are ignored (Haase & Smith, 1989*a*, *b*; Feliks 1988).

The thermodynamic energy equation is

$$\frac{\partial \sigma}{\partial t} + u\frac{\partial \sigma}{\partial x} + w\frac{\partial \sigma}{\partial z} = 0. \tag{2.4}$$

Here $\sigma = \sigma' + N^2 z$, $N^2 = (g/\theta_m)\partial\bar{\theta}/\partial z$ is the Brunt–Väisälä frequency of the atmosphere, θ_m and $\bar{\theta}$ are the mean and reference potential temperature and

$$\sigma = \frac{\rho g}{\rho_m} = \frac{g\theta}{\theta_m} \tag{2.5}$$

is the buoyancy force; θ is the potential temperature perturbation from its value at the lower boundary.

As the fluid is incompressible a streamfunction will be introduced, where

$$u = -\frac{\partial \psi}{\partial z}, \quad w = \frac{\partial \psi}{\partial x}. \tag{2.6}$$

Cross-differention of (2.1) and (2.2) will eliminate the pressure, leading to the vorticity equation

$$\frac{\partial \zeta}{\partial t} + u\frac{\partial \zeta}{\partial x} + w\frac{\partial \zeta}{\partial z} = \frac{\partial \sigma}{\partial x}, \tag{2.7}$$

$$\zeta = \frac{\partial w}{\partial x} - \frac{\partial u}{\partial z} = \nabla^2 \psi. \tag{2.8}$$

To solve analytically the above nonlinear equations we assume that the speed of the front is constant and the front maintains its structure.

The transformation of the x-coordinate to the $(s = x - ct)$-coordinate, where c is the front speed, enables us to eliminate the time derivative from equations (2.4) and (2.7), i.e.

$$J(\psi + cz, \zeta) - \frac{\partial \sigma}{\partial s} = 0, \tag{2.9}$$

$$J(\psi + cz, \sigma) = 0, \tag{2.10}$$

where J is the Jacobian operator.

https://doi.org/10.1017/S0022112000001488 Published online by Cambridge University Press

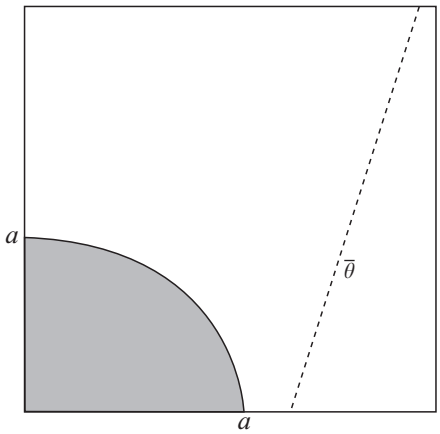


FIGURE 1. Diagram of the frontal region in the moving coordinates (s, z). The shaded quarter of circle on the left-hand side represents the frontal area whose radius is a. The undisturbed potential temperature profile is shown on the right-hand side.

In figure 1, a diagram of the frontal region in the moving coordinate system is shown. We look for a solution to (2.9) and (2.10) in the region $z > 0$, $s > 0$. This solution has to fulfil the following boundary conditions: (i) $w = o$ on $z = 0$, and (ii) for the horizontal velocity, u, a free-slip condition is assumed. The disturbance tends to zero as

$$x \to \infty, \text{ i.e. } u \to U, w \to 0,$$

$$\psi \to -Uz \quad \text{and} \quad \frac{\partial \sigma}{\partial z} \to N^2. \tag{2.11}$$

On the front boundary $r = a$ (figure 1), $\psi + cz = 0$. This indicates that there is no mass flux through the front boundary. On this boundary ψ, u, w, and σ are continuous. Because the Jacobian in (2.10) vanishes, there is an arbitrary functional dependence between $\psi + cz$ and σ. Assume this function is piecewise-linear, i.e.

$$\left.\begin{aligned} \sigma &= \gamma_I(\psi + cz), \quad r < a, \\ \sigma &= \gamma_E(\psi + cz), \quad r > a. \end{aligned}\right\} \tag{2.12a}$$

According to (2.4) the isolines of the buoyancy, σ, coincide with the streamlines, $\psi + cz$, due to the assumption of adiabatic flow in our model. In (2.12a) γ_I and γ_E ($\gamma_{I,E}$ below) are coefficients of proportionality between the streamlines, $\psi + cz$ and the buoyancy isolines inside and outside the density current. A further interpretation of γ_I and γ_E can be obtained by differentiating (2.12a) with respect to x; we obtain

$$\frac{\partial \sigma}{\partial x} = \gamma_{I,E} \frac{\partial}{\partial x}(\psi + cz) = \gamma_{I,E} w, \tag{2.12b}$$

i.e. increasing the horizontal gradient of the streamlines by w results in increasing the horizontal gradient of the buoyancy by $\gamma_{I,E} w$. This gradient generates vorticity at a rate $\gamma_{I,E}\, w$ (see (2.7)). In our inviscid model the tilting of the buoyancy surfaces is the only source generating vorticity.

In (2.12a) the transition from one portion of the broken line to another is a function of the distance r from the coordinate origin, rather than the value of the argument

https://doi.org/10.1017/S0022112000001488 Published online by Cambridge University Press

$\psi + cz$. Thus a has to be chosen in the following manner:

$$\left.\begin{aligned} \psi + cz < 0, \quad r < a, \\ \psi + cz > 0, \quad r > a. \end{aligned}\right\} \tag{2.13}$$

This condition also ensures continuity of the buoyancy, σ, as we move from one portion of the broken line to another. The other choice $\psi + cz > 0$ (when $r < a$) leads to weak horizontal winds in the front since $u = -\partial\psi/\partial z < c$. We note that the shape of the front as given by the curve $\psi + cz = 0$ is an assumption of the theory to make the problem mathematically tractable. Near the stagnation point this front, has an angle of 90° between the frontal interface and the horizontal plane. In previous analytical solutions (Benjamin 1968; Xu 1992; Liu & Moncrieff 1996; Xu *et al.* 1996) the angle at the stagnation point is 60°. This difference in the angle at the stagnation point between our solution and the previous solutions can be attributed to the differences in the properties of the solutions. In our solution, pressure and its first derivative, and velocity and density are continuous at the interface while in the previous solutions only the pressure is continuous. In our solution there is intensive circulation with strong vorticity inside the gravity current and the dynamics is non-hydrostatic. In the previous studies the flow inside the gravity current is motionless (in a relative frame of reference) so the effect of the dynamics is excluded. Thus the hydrostatic approximation is valid and so the pressure on the interface from inside the front is determined. The study of Xu & Moncrieff (1994) considers circulation in the head with constant vorticity. Their analysis shows that the circulation in the gravity current does not influence the propagation. This conclusion can be derived directly from the vorticity equation (2.7) since the nonlinear advection terms are zero when the vorticity is constant. We also note that Jirka & Arita (1987) showed that a 60° angle is obtained when the vorticity on both sides of the front is zero or constant, as is the case in the previous studies. But for more complicated vorticity structure near the stagnation point the angle can be larger than 60° and the propagation depends on the vorticity structure in the gravity current head, as will be shown in § 5. In the solution of Jirka & Arita (1987) the vorticity is singular at the stagnation point and so it is valid only for viscid flow. In our solution the vorticity is not singular, even at the stagnation point.

Substituting (2.11) into (2.12*a*) gives

$$\sigma \to \gamma_E(c - U)z = N^2 z \quad \text{as} \quad s \to \infty. \tag{2.14}$$

Because $N^2 > 0$ and $c - U > 0$, we find

$$\gamma_E > 0. \tag{2.15}$$

Then substituting (2.12) and (2.9) we obtain

$$\left.\begin{aligned} J(\psi + cz, \zeta - \gamma_I z) = 0, \quad r < a, \\ J(\psi + cz, \zeta - \gamma_E z) = 0, \quad r > a. \end{aligned}\right\} \tag{2.16}$$

Since the Jacobian in (2.16) vanishes there is an arbitrary functional dependence between $\psi + cz$ and

$$\zeta - \gamma_I z, \quad r < a,$$

$$\zeta - \gamma_E z, \quad r > a,$$

https://doi.org/10.1017/S0022112000001488 Published online by Cambridge University Press

assuming this function is piecewise-linear, i.e.

$$\left.\begin{aligned} \nabla^2\psi - \gamma_I z &= -k^2(\psi + cz), \quad r < a, \\ \nabla^2\psi - \gamma_E z &= \pm p^2(\psi + cz), \quad r > a. \end{aligned}\right\} \tag{2.17}$$

According to (2.16) the isolines of the potential vorticity, $\zeta - \gamma_I z$, coincide with the streamlines $\psi + cz$. The parameters $-k^2$ and p^2 are coefficients of proportionality between the potential vorticity and the streamlines inside and outside the gravity current. The change of the vorticity, $\nabla^2\psi$, of a moving particle (along a streamline) is due to its vertical displacement. As the particle moves upward a distance z it gains vorticity $\gamma_{I,E} z$ (inside and outside the front), since ascent in a stratified environment causes tilting of the buoyancy surfaces, as shown above in (2.12*b*). The sign of p^2 in (2.17) is determined as follows: as $s \to \infty$, $\nabla^2\psi \to 0$ and $\psi \to -Uz$, thus (2.17) becomes

$$-\gamma_E = \pm p^2(c - U) \quad \text{as} \quad s \to \infty. \tag{2.18}$$

Since $\gamma_E > 0$, $c - U > 0$ only the negative sign is admitted, i.e.

$$\frac{\gamma_E}{p^2} = c - U. \tag{2.19a}$$

From (2.14) and (2.19*a*) we find

$$p^2 = \frac{N^2}{(c-U)^2}. \tag{2.19b}$$

Thus

$$Fr = \frac{1}{pa} = \frac{c-U}{Na} \tag{2.19c}$$

can be considered the Froude number of the problem. For a constant Froude number, increasing the front height, a, or the atmosphere stability, N, results in an increase in the front speed relative to the synoptic wind.

Equations (2.17) take the form

$$\left.\begin{aligned} \nabla^2\psi + k^2\psi_I &= (\gamma_I - k^2 c)z, \quad r < a, \\ \nabla^2\psi + p^2\psi_I &= (\gamma_E - p^2 c)z, \quad r > a. \end{aligned}\right\} \tag{2.20}$$

The complete solution to (2.20) in polar coordinates $s = r\cos\alpha$, $z = r\sin\alpha$, is given by

$$\left.\begin{aligned} \psi &= \frac{\gamma_I a}{k^2}\left[-\frac{J_1(kr)}{J_1(ka)} + \frac{r}{a}\right]\sin\alpha - cr\sin\alpha, \quad r < a, \\ \psi &= (c-U)a\left[-\frac{Y_1(pr)}{Y_1(pa)} + \frac{r}{a}\right]\sin\alpha - cr\sin\alpha, \quad r > a, \end{aligned}\right\} \tag{2.21}$$

as explained in the Appendix. Here J_1 and Y_1 are first-order Bessel functions of the first and second kind. The ranges of ka and pa and the formulation for γ_I are also derived in the Appendix and are given by

$$0 < ka < 3.8317, \quad 0 < pa < 2.03, \tag{2.22}$$

and

$$\gamma_I = (c-U)kp\,\frac{Y_2(pa)}{Y_1(pa)}\,\frac{J_1(ka)}{J_2(ka)} = Nk\,\frac{Y_2(pa)}{Y_1(pa)}\,\frac{J_1(ka)}{J_2(ka)}. \tag{2.23}$$

https://doi.org/10.1017/S0022112000001488 Published online by Cambridge University Press

3. Potential temperature

In the region $r < a$ using (2.12a) and (2.21) we get (see also Feliks 1988)

$$\sigma = \frac{\gamma_I^2 a}{k^2}\left[-\frac{J_1(kr)}{J_1(ka)} + \frac{r}{a}\right]\sin\alpha. \tag{3.1}$$

Substituting (2.5) and (2.23) into (3.1) we obtain

$$\theta = \frac{\theta_m}{g}\frac{(c-U)^2}{a}\left\{\left[pa\frac{Y_2(pa)}{Y_1(pa)}\frac{J_1(ka)}{J_2(ka)}\right]^2\left[-\frac{J_1(kr)}{J_1(ka)} + \frac{kr}{ka}\right]\sin\alpha\right\}. \tag{3.2}$$

or

$$\theta = \frac{\theta_m}{g}N^2 a\left\{\left[\frac{Y_2(pa)}{Y_1(pa)}\frac{J_1(ka)}{J_2(ka)}\right]^2\left[-\frac{J_1(kr)}{J_1(ka)} + \frac{kr}{ka}\right]\sin\alpha\right\}. \tag{3.3}$$

In the region $r > a$ using (2.12a) and (2.21) we get

$$\sigma = \gamma_E(c-U)a\left[-\frac{Y_1(pr)}{Y_1(pa)} + \frac{(pr)}{(pa)}\right]\sin\alpha. \tag{3.4}$$

Substituting (2.5) and (2.19a) into (3.4) we obtain

$$\theta = \frac{\theta_m}{g}\frac{(c-U)^2}{a}\left\{(pa)^2\left[-\frac{Y_1(pr)}{Y_1(pa)} + \frac{pr}{pa}\right]\sin\alpha\right\} = \frac{\theta_m}{g}N^2 a\left[-\frac{Y_1(pr)}{Y_1(pa)} + \frac{pr}{pa}\right]\sin\alpha. \tag{3.5}$$

The expressions in the curly brackets in (3.2), (3.3) and (3.5) are non-dimensional and describe the structure of the potential temperature as a function of ka and pa. In figure 2 this function is shown for different values of ka and pa in the non-dimensional coordinates s/a, z/a. In cold fronts, as ka decreases and pa increases there is an increase of the temperature drop in the front. Significant differences in the structure of θ outside the front are observed as a function of pa. For $pa < 1 (Fr > 1)$ no waves appear ahead of the front and the solution in this regime can be considered supercritical, in the sense that the phase speed of the gravity waves is less than the speed of the front. For $pa > 1 (Fr < 1)$ waves appear ahead of the front and this regime can be considered as subcritical in the sense that the phase speed of the gravity waves is greater than the speed of the front. These two regimes of the solution were suggested by Haase & Smith (1989a, b). In their numerical simulations they show the evolution of the solution in each regime. As pa increases further the horizontal and vertical scales of the nonlinear wave decrease and its amplitude increases.

In cold fronts, unstable profiles of θ are obtained in the lower layers in our model, particularly when the atmospheric stability is low. These unstable profiles are due to lack of vertical friction in our model. Including this mechanism would result in neutral profiles in the lower part of the front and consequently in strong horizontal temperature gradients near the ground.

The maximum of $|\theta|$ in the front ($r < a$), θ_{max}, is determined by the maximum of the structure function

$$\left[\frac{J_1(ka)}{J_2(ka)}\right]^2\left[-\frac{J_1(kr)}{J_1(ka)} + \frac{kr}{ka}\right]. \tag{3.6}$$

(Note that this structure function is different from that shown in figure 2 and (3.2)

https://doi.org/10.1017/S0022112000001488 Published online by Cambridge University Press

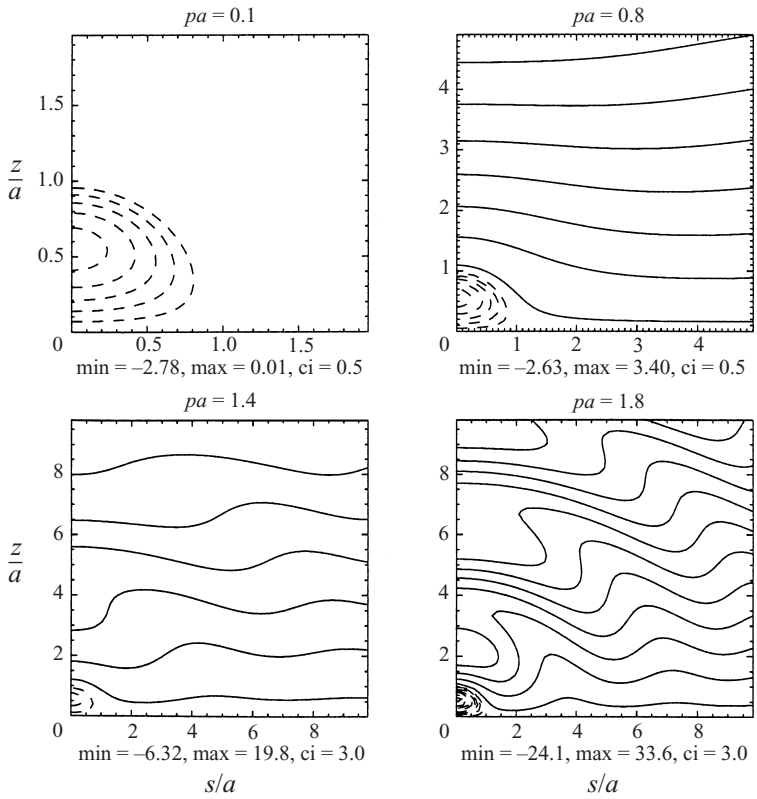


FIGURE 2. Isolines of the functional structure of the buoyancy and potential temperature for various values of pa and $ka = 2$, as function of the non-dimensional moving coordinates s/a, z/a.

and (3.3)). The amplitude of this structure function is

$$D = \frac{\theta_m}{g} N^2 a \left[\frac{Y_2(pa)}{Y_1(pa)}\right]^2 = \frac{\theta_m}{g}\frac{(c-U)^2}{a}\left[pa\frac{Y_2(pa)}{Y_1(pa)}\right]^2. \tag{3.7}$$

In figure 3 the maximum of the structure function (3.6) in the cold front region is shown as a function of ka (note that in $r < a$ the structure function is only a function of ka). To determine the value of ka one has to know the atmospheric stability, N, and the speed of the front, c, relative to the undisturbed synoptic wind speed, U, the height of the front, a, and the maximum drop of temperature due to the passage of the front. From (2.19b) we find p and can calculate the amplitude D, (3.7), and using figure 3 ka is determined.

The temperature drop due to the passage of the cold front is proportional to $(c-U)^2$ and inversely proportional to the front height a (3.2). Some values of θ_{max}, c, U, N, and pa are given in table 1, as obtained from our model.

The integral of (3.2) over the front area is

$$\iint \theta \,\mathrm{d}A = \frac{\theta_m}{g}\frac{(c-U)^2}{a}\left\{\left[pa\frac{Y_2(pa)}{Y_1(pa)}\frac{J_1(ka)}{J_2(ka)}\right]^2 \int_0^{\pi/2}\int_0^a \left[-\frac{J_1(kr)}{J_1(ka)} + \frac{kr}{ka}\right]\sin\alpha \,\mathrm{d}r\,\mathrm{d}\alpha\right\}. \tag{3.8}$$

https://doi.org/10.1017/S0022112000001488 Published online by Cambridge University Press

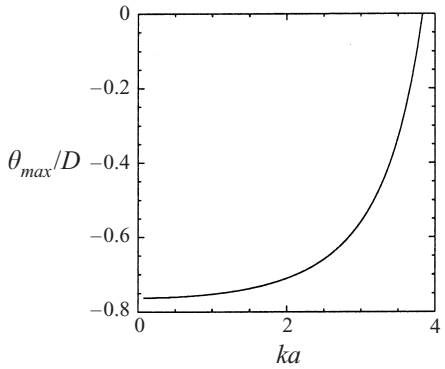


FIGURE 3. The maximum potential temperature change due to the passage of the front, normalized by D (equation (3.7)) as a function of ka.

Using the identity $yJ_1(y) = -yJ_0'(y)$ and integrating by parts we obtain

$$(c-U)^2 = \frac{\pi g a \iint \theta \, \mathrm{d}A}{4\theta_m \left[pa \dfrac{Y_2(pa)}{Y_1(pa)} \dfrac{J_1(ka)}{J_2(ka)}\right]^2 \left[\left(\dfrac{J_0(ka)}{J_1(ka)} H_1(ka) - H_0(ka)\right) \dfrac{\pi}{2ka} + \dfrac{1}{3}\right]}, \tag{3.9}$$

where H_0 and H_1 are Struve functions.

From the mean value theorem for definite integrals, we have

$$\iint \theta \, \mathrm{d}A = \theta(\bar{x}) \frac{\pi a^2}{4}, \tag{3.10}$$

where $\bar{x}$ is a point in the front, and so

$$(c-U)^2 = \frac{4\theta(\bar{x}) g a}{\theta_m \left[pa \dfrac{Y_2(pa)}{Y_1(pa)} \dfrac{J_1(ka)}{J_2(ka)}\right]^2 \left[\left(\dfrac{J_0(ka)}{J_1(ka)} H_1(ka) - H_0(ka)\right) \dfrac{\pi}{2ka} + \dfrac{1}{3}\right]}, \tag{3.11}$$

i.e. the square of the speed of the gravity current relative to the synoptic wind is proportional to the mean drop of θ over the front area, $\theta(\bar{x})$, times the front height, a, when ka and pa are kept constant. This result, within constant factors, is similar to that found by Benjamin (1968) and Feliks (1988). In the real atmosphere the relation $(c-U)^2 = F^2 \Delta\theta g a/\theta_m$ is widely used with a constant F^2. Wakimoto (1982) used $F^2 = 0.57$, unlike the value 2 found by Benjamin (1969); for more discussion on the value of F^2 see Liu & Moncrieff (1996). We assume that the large difference in F^2 between different studies results from the different environmental conditions as expressed in (3.11). From (3.5) we obtain that θ outside the front ($r > a$) is a function of pa, $c-U$ and a, but not a function of ka. On the other hand, θ inside the front is also function of ka; increasing ka results in decreasing θ. Thus fronts with the same speed and height can have different θ (as shown in figure 3). So the speed of the front is also a function of the flow in the front, i.e. the balance between the nonlinear advection term and the horizontal gradient of the buoyancy, as will be discussed below in § 5. This result is different from that of Benjamin (1968), and Liu & Moncrieff (1996); in both cases the speed of the front is only a function of the temperature drop in the front and its height. This difference is due to the fact that the flow in the front is motionless in the relative frame. Moncrieff & So (1989) examined

https://doi.org/10.1017/S0022112000001488 Published online by Cambridge University Press

gravity currents when flow and vorticity are observed in the cold front and showed that the solution strongly depends on both flow and vorticity.

4. The winds

An analytical expression for the horizontal and vertical velocities can be obtained from (2.6):

$$\left.\begin{aligned} u - c &= -\frac{\partial \psi}{\partial z} - c = -\left(\frac{\partial \psi}{\partial r}\frac{\partial r}{\partial z} + \frac{\partial \psi}{\partial \alpha}\frac{\partial \alpha}{\partial z}\right) - c, \\ w &= \frac{\partial \psi}{\partial s} = \frac{\partial \psi}{\partial r}\frac{\partial r}{\partial s} + \frac{\partial \psi}{\partial \alpha}\frac{\partial \alpha}{\partial s}, \end{aligned}\right\} \tag{4.1}$$

using (2.21) and the trigonometric identity $\arctan'(x) = 1 + (1 + x^2)$. After some mathematical manipulation we have:
for $r < a$

$$u - c = (c - U)\left\{pa\frac{Y_2(pa)}{Y_1(pa)}\frac{1}{J_2(ka)}\left[\frac{J_1(kr)}{kr} - J_2(kr)\sin^2\alpha - \frac{J_1(ka)}{ka}\right]\right\}, \tag{4.2}$$

$$w = (c - U)\left\{pa\frac{Y_2(pa)}{Y_1(pa)}\frac{J_2(kr)}{J_2(ka)}\sin\alpha\cos\alpha\right\}; \tag{4.3}$$

for $r > a$

$$u - c = (c - U)\left\{\frac{pa}{pr}\frac{Y_1(pr)}{Y_1(pa)} - pa\frac{Y_2(pr)}{Y_2(pa)}\sin^2\alpha - 1\right\}, \tag{4.4}$$

$$w = (c - U)\left\{pa\frac{Y_2(pr)}{Y_1(pa)}\sin\alpha\cos\alpha\right\}. \tag{4.5}$$

The expressions in curly brackets in (4.2)–(4.5) are non-dimensional and describe the structure of the horizontal and vertical velocities. The dimensional velocities are proportional to $c - U$. In figures 4 and 5 the structure functions are shown for $u - c$ and w (horizontal and vertical respectively), in the non-dimensional coordinates s/a, z/a, for different values of pa.

In the horizontal velocity, u, (figure 4) for small pa an abrupt change in $u - c$ is observed as we cross the front line $r = a$. As pa increases, the wind intensity inside the front increases. As pa increases, the wind speed outside the front also increases. For $pa > 1$, u has an undular pattern, most prominent above the front. The undular pattern intensifies as pa increases. A return current is observed in the front at altitudes above the front centre ($z/a > 0.5$). Some values of the maximum and minimum of the horizontal wind speed in the front and outside of it are given in table 1.

In the vertical velocity (figure 5) upward motions are observed over the front. The height at which the maximum is found is the boundary between the convergence and divergence zones observed in the horizontal velocity. This maximum observed along the ray begins at the origin at an angle of 45°. For $pa > 1$ outside the front, cells of upward and downward velocities are observed ahead of the front in the undulating region. Upward cells are observed in the convergence zones and downward cells in the divergence zones. Some values of the maximum speed of the vertical velocity inside and outside the front are also given in table 1.

https://doi.org/10.1017/S0022112000001488 Published online by Cambridge University Press

https://doi.org/10.1017/S0022112000001488 Published online by Cambridge University Press

U ($\mathrm{m\,s^{-1}}$)	c ($\mathrm{m\,s^{-1}}$)	$\lvert\theta_{max}\rvert$ (°C)	pa	u_{max} ($\mathrm{m\,s^{-1}}$)	u_{min} ($\mathrm{m\,s^{-1}}$)	w_{max} ($\mathrm{m\,s^{-1}}$)	w_{min} ($\mathrm{m\,s^{-1}}$)	$N \times 10^3$ ($\mathrm{s^{-1}}$)	$(k^2c - \gamma_I) \times 10^5$ ($\mathrm{m^{-1}\,s^{-1}}$)	$\gamma_I \times 10^5$ ($\mathrm{m^{-1}\,s^{-1}}$)	$\gamma_E \times 10^6$ ($\mathrm{m^{-1}\,s^{-1}}$)
−3	2	3.0	0.1	7.9	−7.9*	4.9	0	0.71	−5.0	6.6	0.1
−3	2	2.9	0.8	7.8	−6.9*	4.6	−0.8*	5.7	−4.8	6.4	6.5
−3	2	3.2	1.4	11	−12.3*	7.5	−6.6*	10.0	4.8	0.9	20.0
2	4	0.5	0.1	6.4	0.1*	2.0	0	0.71	0.6	2.6	0.04
2	4	3.9	1.8	11	−6.8*	5.5	−3.0	13.0	−4.5	7.8	1.3

TABLE 1. In this table the front height is $a = 700\,\mathrm{m}$, and $ka = 2$; u_{max}, u_{min}, w_{max} and w_{min} are the maximum and minimum of u and w respectively.
*Values obtained outside the front.

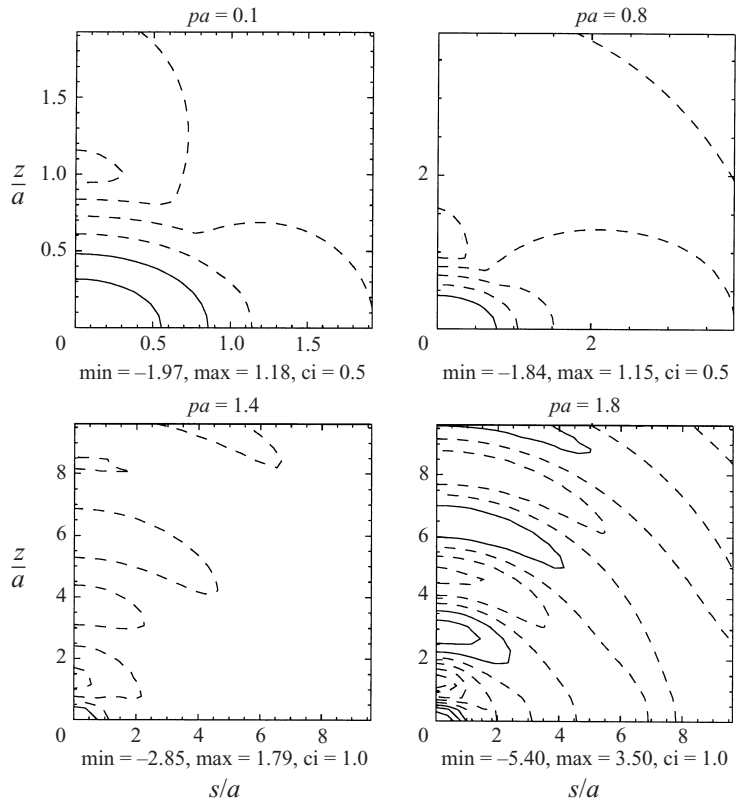


FIGURE 4. Isolines of the structure function of the horizontal velocity relative to the front speed for various values of pa and $ka = 2$, as a function of the non-dimensional moving coordinates s/a, z/a.

5. The causes of propagation

The causes of propagation of the front and the nonlinear gravity wave ahead of it are studied below in terms of the vorticity equation. An analytical expression for the vorticity can be obtained from (2.1):
for $r < a$

$$\zeta = \nabla^2\psi = -k^2\psi + (\gamma_I - k^2 c)z. \tag{5.1}$$

Substituting ψ form (2.21) into (5.1) we obtain

$$\zeta = \gamma_I a \frac{J_1(kr)}{J_1(ka)} \sin\alpha = \frac{(c-U)}{a}\left\{pa\frac{Y_2(pa)}{Y_1(pa)} ka \frac{J_1(kr)}{J_2(ka)}\sin\alpha\right\}; \tag{5.2}$$

γ_I is given in (2.23).
For $r > 0$

$$\zeta = \nabla^2\psi = -p^2\psi + (\gamma_E - p^2 c)z. \tag{5.3}$$

Substituting ψ from (2.21) into (5.3) we obtain

$$\zeta = \frac{c-U}{a}\left\{(pa)^2 \frac{Y_1(pr)}{Y_1(pa)}\sin\alpha\right\}. \tag{5.4}$$

In the frontal region $r < a$ the vorticity has a positive sign and its maximum is obtained at $\alpha = \pi/2$. The structure function of the vorticity is given in the curly brackets of (5.2) and (5.4) and is shown in figure 6 for several values of pa. The

https://doi.org/10.1017/S0022112000001488 Published online by Cambridge University Press

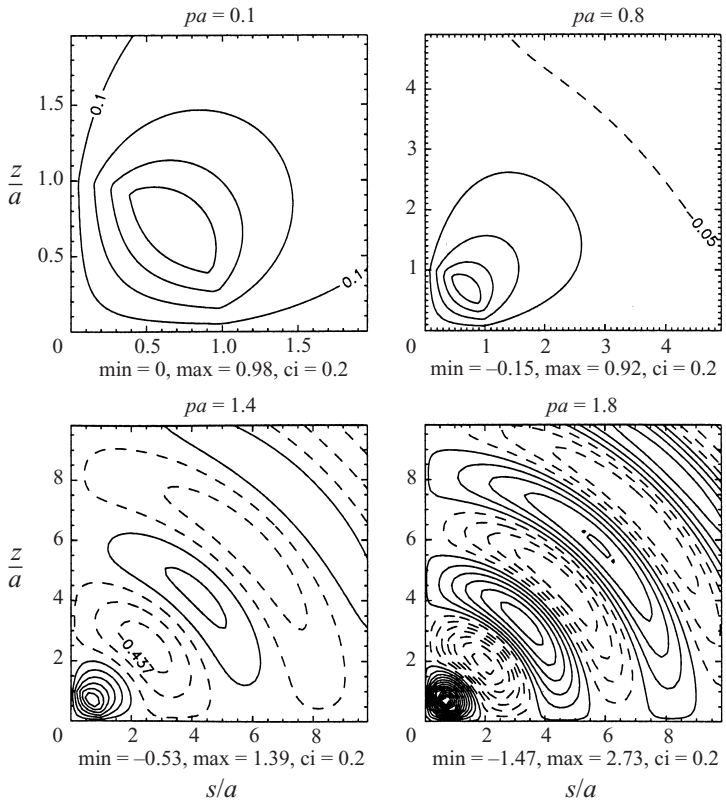


FIGURE 5. Isolines of the structure function of the vertical velocity for various values of pa and $ka = 2$, as a function of the non-dimensional moving coordinates s/a, z/a.

dimensional vorticity is proportional to $(c-U)/a$. As pa increases, the vorticity inside the front increases. As pa increases the vorticity outside the front increases and for $pa > 1$ cells of negative and positive vorticity appear ahead of the front in the undulating region (figures 2, 4 and 5).

Examination of the vorticity equation (2.7) shows that two terms cause the changes in the vorticity: the nonlinear advective term $-J(\psi,\zeta)$ and the horizontal gradient of buoyancy (or potential temperature) $\partial\sigma/\partial x$. A positive horizontal gradient of the buoyancy tends to increase the vorticity, while a negative one decreases it. The analytical expressions for these two terms in the front are

$$-J(\psi,\zeta) = -J[\psi, -k^2\psi + (\gamma_I - k^2 c)z] = \frac{\partial\psi}{\partial x}(k^2c - \gamma_I) = w(k^2c - \gamma_I), \tag{5.5}$$

$$\frac{\partial\sigma}{\partial x} = \frac{\partial}{\partial x}[\gamma_I(\psi + cz)] = \frac{\partial\psi}{\partial x}\gamma_I = w\gamma_I. \tag{5.6}$$

The sum of the two terms gives

$$\frac{\partial\zeta}{\partial t} = wk^2c \tag{5.7}$$

Since w is positive everywhere in the frontal area, the right-hand side of (5.7) is positive and causes the eastward propagation of the front.

The contribution of the nonlinear advective term to the vorticity depends on the sign of $k^2c - \gamma_I$. When this sign is negative, the advection term decreases the vorticity

https://doi.org/10.1017/S0022112000001488 Published online by Cambridge University Press

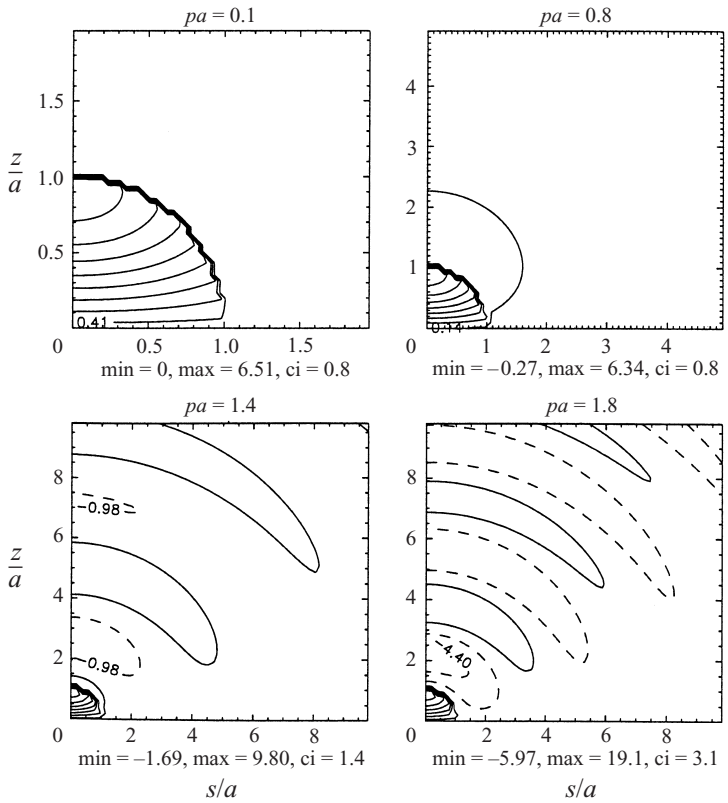


FIGURE 6. Same as figure 5 but for the vorticity.

and so inhibits the propagation of the front, and vice versa when its sign is positive. To evaluate this coefficient we substitute (2.21) for γ_I:

$$k^2c - \gamma_I = \frac{kc}{a}\left[ka - \frac{(c-U)}{c}pa\frac{Y_2(pa)}{Y_1(pa)}\frac{J_1(ka)}{J_2(ka)}\right]. \tag{5.8}$$

Across the front, $\partial\sigma/\partial x > 0$, and this term tends to propagate the front eastward. Values of the coefficient (5.8) are given in figure 7 as a function of ka and $(c-U)/c$ for $pa = 0.1$ and 1.8 ($(c-U)/c < 1$ refers to $U > 0$ and $(c-U)/c > 1$ refers to $U < 0$). Some values of $k^2c - \gamma_I$ are given in table 1. In most of the cases the advection term has a negative sign due to advection of particles with low vorticity into a region of higher vorticity, and so this term slows the eastward propagation of the front. When the buoyancy in the front is very low the advection term is positive. This is due to the advection of particles with high vorticity into the region of lower vorticity. Thus the advection tends to speed up the propagation.

Outside the front, $r > a$, the analytical expressions for the relevant terms of the vorticity equations are

$$-J(\psi,\zeta) = -J[\psi, -p^2\psi + (\gamma_E - p^2c)] = \frac{\partial\psi}{\partial x}(p^2c - \gamma_E) = w(p^2c - \gamma_E) = wp^2U, \tag{5.9}$$

$$\frac{\partial\sigma}{\partial x} = \frac{\partial}{\partial x}[\gamma_E(\psi + cz)] = \frac{\partial\psi}{\partial x}\gamma_E = wp^2(c-U). \tag{5.10}$$

https://doi.org/10.1017/S0022112000001488 Published online by Cambridge University Press

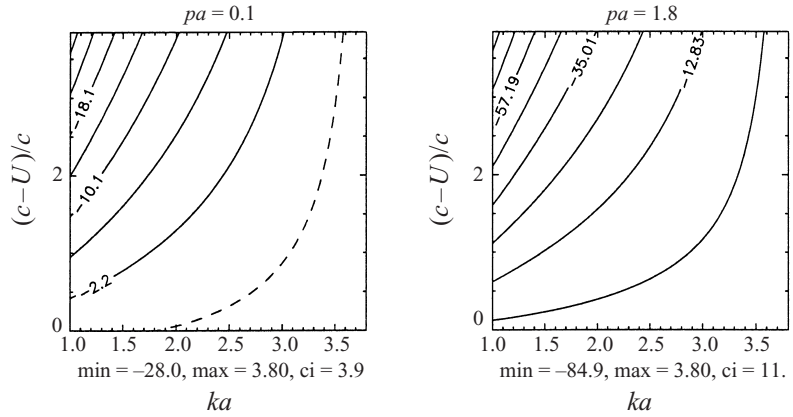


FIGURE 7. Isolines of $\left[ka - \dfrac{(c-U)}{c} pa \dfrac{Y_2(pa)}{Y_1(pa)} \dfrac{J_1(ka)}{J_2(ka)}\right]$, i.e. the coefficient of the nonlinear advective term normalized by kc/a (see (5.8)) as a function of $(c-U)/c$ and ka.

Here the sum of the two terms gives

$$\frac{\partial \zeta}{\partial t} = wp^2 c. \tag{5.11}$$

Propagation direction here is more complex: the right-hand side of (5.10) has the same sign as w. Examining figures 5 and 6 (for $pa = 1.4$ and 1.8) we find that the cells of positive w overlap most of the parts where ζ decreases as function of x, and cells of negative w overlap most of the parts where ζ increases as function of x. Thus the right-hand side of (5.10) tends to speed up the propagation of the disturbance of the gravity wave ahead of the front. This result can be deduced directly from the functional properties of ζ which behaves like $Y_1(pr)$, (5.4), and that of w which behaves like $Y_2(pr)$, (4.5). The nodes of $Y_2(pr)$ are very close to the extrema of $Y_1(pr)$.

The right-hand side of (5.9) depends on the sign of U. When $U > 0$, i.e. when the synoptic wind is blowing in the direction of the propagation, this term has the same sign as (5.10) and so tends to speed up the propagation of the disturbance ahead of the front. When $U < 0$, i.e. the synoptic wind blows opposite to the direction of propagation, this term has the opposite sign to that of (5.10) and so tends to slow the propagation of the disturbance ahead of the front.

6. Concluding remarks

An analytical solution to the nonlinear equations of motion and the thermodynamic energy equation describes a cold front propagating in stable atmosphere. This solution assumes that the front has constant speed of propagation, and that it maintains its structure. This is an extension of Feliks (1988), where a solution was found for unstable and neutral atmospheres. This solution is different from the previous analytical solutions of gravity currents in several aspects. Here, the shape of the front is prescribed, and the density and velocity are determined by the solution and are continuous on the interface; only their derivative is discontinuous. In the previous studies the density is prescribed, the shape of the front and the velocity are determined by the solution, and the velocity and density are discontinuous on the interface. In our solution there is intensive circulation with strong vorticity inside the gravity current and the dynamics is non-hydrostatic. Such circulation is observed in the atmospheric gravity currents.

https://doi.org/10.1017/S0022112000001488 Published online by Cambridge University Press

The solution has two regimes: (i) A supercritical regime when the Froude number of the problem is $Fr = (c - U)/Na = 1/pa > 1$. The cold front is local and is similar to that found in a neutral or unstable atmosphere. (ii) A subcritical regime when $Fr = 1/pa < 1$. Ahead of the front a disturbance of the nonlinear gravity wave is found. The horizontal scale of the wave decreases and its amplitude increases as Fr decreases. The thermal, velocity, and vorticity fields can be described by non-dimensional structure functions of the two parameters pa and ka. The amplitude of the structure functions is proportional to $(c - U)^2/a$ for the thermal field, to $(c - U)$ for the velocity field and to $(c - U)/a$ for the vorticity field.

The propagation is studied in terms of the vorticity equation. The horizontal gradient of the buoyancy term always tends to propagate the cold front. The nonlinear advection term (in most of the cases) tends to slow the propagation. The propagation of the disturbance of nonlinear gravity waves ahead of the front (when $Fr < 1$) in most of the domain is due to the buoyancy term. The nonlinear advection term tends to slow the propagation when the synoptic wind blows in the opposite direction to that of propagation, and vice versa when the synoptic wind blows in the direction of propagation. The square of the speed of the front relative to the synoptic wind is proportional to

$$\frac{2\theta(\bar{x})}{\theta_m} ga,$$

where $\theta(\bar{x})$ is the mean potential temperature drop across the front area and a is the front height. We find that the square of the speed is also strongly dependent on the environmental conditions in the front. This result is widely used in the interpretation of observed gravity currents. The constant of proportionality varies greatly between different studies. We attribute these differences to the different environmental conditions in the observations. Moncrieff & So (1989) also found a strong dependence of the gravity current speed on the flow and vorticity in the front. Liu & Moncrieff (1996) assumed no flow in the front; thus they found faster propagation, since the tendency of the nonlinear advection to slow the propagation is absent from their model.

The analytical solution presented here does not include important physical processes such as eddy diffusivity. Including such processes will probably change the unstable thermal field in the lower part of the front to neutral stratification. Changing the slip condition in the lower boundary to a non-slip condition will affect the velocity field near the ground and can influence the speed of the front, as shown by Haase & Smith (1989*a*, *b*).

The stability regimes of this analytical solution to small perturbations are left for further study.

I am grateful to Dr Y. Alexander for careful reading of the manuscript.

Appendix

In polar coordinates (2.20) becomes

$$\left.\begin{aligned} \frac{1}{r}\frac{\partial}{\partial r}\left(r\frac{\partial \psi}{\partial r}\right) + \frac{1}{r^2}\frac{\partial^2 \psi}{\partial r^2} + k^2\psi &= (\gamma_I - k^2) r \sin\alpha, \quad r < a, \\ \frac{1}{r}\frac{\partial}{\partial r}\left(r\frac{\partial \psi}{\partial r}\right) + \frac{1}{r^2}\frac{\partial^2 \psi}{\partial r^2} + p^2\psi &= (\gamma_E - p^2) r \sin\alpha, \quad r > a. \end{aligned}\right\} \tag{A 1}$$

https://doi.org/10.1017/S0022112000001488 Published online by Cambridge University Press

A particular solution of (A 1) is

$$\psi_{NH} = \frac{\gamma - l^2 c}{l^2} r \sin\alpha. \tag{A 2}$$

where $l = k$ or p and $\gamma = \gamma_I$ or γ_E. The solution of the homogeneous equation is obtained by the separation of variables:

$$\left.\begin{aligned} \psi_H &= f(r)h(\alpha), \\ \frac{r}{f}\frac{\partial}{\partial r}\left(r\frac{\partial f}{\partial r}\right) + r^2 l^2 = 1 &= -\frac{1}{h}\frac{\partial^2 h}{\partial \alpha^2}. \end{aligned}\right\} \tag{A 3}$$

Thus

$$h(\alpha) = \sin\alpha, \quad f(r) = AJ_1(lr) + BY_1(lr) \tag{A 4}$$

where J_1 and Y_1 are first order Bessel functions of the first and second kind.

For $r < a$ $B = 0$ since as $r \to 0$ $Y_1(lr) \to -\infty$, i.e.

$$\psi = \left(A_I J_1(kr) + \frac{\gamma_I - ck^2}{k^2} r\right) \sin\alpha \tag{A 5}$$

Utilizing the boundary condition on $r = a$

$$\psi + cz = \psi + ca\sin\alpha = 0, \tag{A 6}$$

we obtain

$$A_I = -\frac{\gamma_I}{k^2}\frac{a}{J_1(ka)}, \tag{A 7}$$

$$\psi = \frac{\gamma_I a}{k^2}\left[-\frac{J_1(kr)}{J_1(ka)} + \frac{r}{a}\right]\sin\alpha - cr\sin\alpha. \tag{A 8}$$

For $r > a$ from (A 3) and (A 4) we obtain

$$\psi = \left(A_E J_1(pr) + B_E Y_1(pr) + \frac{\gamma_E - cp^2}{p^2} r\right)\sin\alpha. \tag{A 9}$$

In § A.1 we show that $A_E = 0$ and

$$\psi = \left(B_E Y_1(pr) + \frac{\gamma_E - cp^2}{p^2} r\right)\sin\alpha. \tag{A 10}$$

Utilizing the boundary condition on $r = a$, (A 6), we obtain

$$B_E = -\frac{\gamma_E}{p^2}\frac{a}{Y_1(pa)} = -(c - U)\frac{a}{Y_1(pa)}, \tag{A 11}$$

$$\psi = (c - U)a\left[-\frac{Y_1(pr)}{Y_1(pa)} + \frac{r}{a}\right]\sin\alpha - cr\sin\alpha. \tag{A 12}$$

From (A 11) and (A 12) we conclude that

$$\left[-\frac{Y_1(pr)}{Y_1(pa)} + \frac{r}{a}\right] > 0 \Rightarrow 0 \leqslant pa \leqslant 2.03. \tag{A 13}$$

It is clear that ψ is continuous on $r = a$. We require continuity for u and w and thus $\partial\psi/\partial r$ must be continuous. After some mathematical manipulation, using the

https://doi.org/10.1017/S0022112000001488 Published online by Cambridge University Press

identities for the derivatives, $Y_1'(y) = Y_1(y)/y - Y_2(y), J_1'(y) = J_1(y)/y - J_2(y)$ we obtain

$$\gamma_I \frac{a}{k}\frac{J_2(ka)}{J_1(ka)} = (c-U)ap\frac{Y_2(pa)}{Y_1(pa)} = Na\frac{Y_2(pa)}{Y_1(pa)} \tag{A 14}$$

or

$$\gamma_I = (c-U)kp\frac{Y_2(pa)}{Y_1(pa)}\frac{J_1(ka)}{J_2(ka)} = Nk\frac{Y_2(pa)}{Y_1(pa)}\frac{J_1(ka)}{J_2(ka)}. \tag{A 15}$$

For $pa \ll 1$, i.e. for the case when the atmosphere tends to neutral stability, and utilizing the approximation (A 24) below we obtain

$$\gamma_I = (c-U)\frac{2k}{a}\frac{J_1(ka)}{J_2(ka)}. \tag{A 16}$$

This result is the same as obtained by Feliks (1988) for a neutral atmosphere, and shows that the extension of the theory to a stable atmosphere is continuous.

In a cold front, the air in the front is cooler than the air ahead of it and so σ in $r < a$ is lower (more negative) than σ in $r > a$. Thus we conclude from (2.12) and (2.13) that $\gamma_I > 0$, and consequently, we can further conclude from (A 15) and (A 16) that

$$J_1(ka) > 0, \quad 0 < ka < 3.8317. \tag{A 17}$$

It is important to note that (A 17) is the only range of ka which is possible for a cold front. For other ranges of ka where $J_1(ka)/J_2(ka) > 0$ for cold fronts, $\psi + cz$ changes its sign in $0 < ra < ka$, but this contradicts (2.13).

A.1. *Demonstration that* $A_E = 0$

From (A 9) we have the general solution for the outer region $r > a$

$$\psi = \left(A_E J_1(pr) + B_E Y_1(pr) + \frac{\gamma_E - cp^2}{p^2}r\right)\sin\alpha. \tag{A 18}$$

Using the boundary condition (A 6) on $r = a$ we find

$$A_E J_1(pa) + B_E Y_1(pa) + \frac{\gamma_E}{p^2}a = 0. \tag{A 19}$$

The continuity of u and w on $r = a$ is consistent with the continuity of $\partial\psi/\partial r$. Thus from (A 18) and (A 8) we obtain

$$\begin{aligned} &pA_E\left(\frac{J_1(pa)}{pa} - J_2(pa)\right) + pB_E\left(\frac{Y_1(pa)}{pa} - Y_2(pa)\right) + \frac{\gamma_E}{p^2} \\ &= kA_I\left(\frac{J_1(ka)}{ka} - J_2(ka)\right) + \frac{\gamma_I}{k^2} \\ &= -J_2(ka)\frac{ka\gamma_I}{k^2 J_1(ka)}. \end{aligned} \tag{A 20}$$

Multiplying (A 20) by a we get

$$A_E J_1(pa) + B_E Y_1(pa) + \frac{\gamma_E}{p^2}a - pa[A_E J_2(pa) + B_E Y_2(pa)] = -ka\frac{\gamma_I}{k^2}\frac{J_2(ka)}{J_1(ka)}. \tag{A 21}$$

Subtracting (A 21) from (A 19) we obtain

$$A_E J_2(pa) + B_E Y_2(pa) = ka\frac{\gamma_I}{k^2}\frac{J_2(ka)}{J_1(ka)} - \frac{\gamma_E}{p^2}a. \tag{A 22}$$

https://doi.org/10.1017/S0022112000001488 Published online by Cambridge University Press

From (A 19) and (A 22) we find

$$A_E = \frac{\left(ka\frac{\gamma_I}{k^2}\frac{J_2(ka)}{J_1(ka)} - \frac{\gamma_E}{p^2}a\right) Y_1(pa) - \frac{\gamma_E}{p^2}aY_2(pa)}{J_2(pa)Y_1(pa) - J_1(pa)Y_2(pa)}. \tag{A 23}$$

For $pa \ll 1$ we can use the following approximations:

$$\left.\begin{aligned} J_1(pa) &\approx \frac{1}{\Gamma(2)}\frac{pa}{2}, \quad J_2(pa) \approx \frac{1}{\Gamma(3)}\frac{(pa)^2}{4}, \\ Y_1(pa) &\approx \frac{\Gamma(1)}{\pi}\frac{2}{pa}, \quad Y_1(pa) \approx -\frac{\Gamma(2)}{\pi}\frac{4}{(pa)^2}. \end{aligned}\right\} \tag{A 24}$$

Thus

$$A_E \approx -\frac{-\left(\frac{ka\gamma_I}{k^2}\frac{J_2(ka)}{J_1(ka)} - \frac{\gamma_E}{p^2}a\right)\frac{\Gamma(1)}{\pi}\frac{2}{pa} + \frac{\gamma_E}{p^2}a\frac{\Gamma(2)}{\pi}\frac{4}{(pa)^2}}{-\frac{1}{\Gamma(3)}\frac{(pa)^2}{4}\frac{\Gamma(1)}{\pi}\frac{2}{pa} + \frac{1}{\Gamma(2)}\frac{pa}{2}\frac{\Gamma(2)}{\pi}\frac{4}{(pa)^2}}. \tag{A 25}$$

From (2.19*a*) and (A 25) we obtain

$$A_E \approx -\frac{-\left(\frac{ka\gamma_I}{k^2}\frac{J_2(ka)}{J_1(ka)} - (c-U)a\right)\frac{\Gamma(1)}{\pi}\frac{2}{pa} + (c-U)a\frac{\Gamma(2)}{\pi}\frac{4}{(pa)^2}}{-\frac{\Gamma(1)}{\Gamma(3)}\frac{pa}{2\pi} + \frac{2}{pa}}. \tag{A 26}$$

As $pa \to 0$, i.e. the atmosphere stratification tends to neutral. (A 26) and (A 9) tend to ∞. But when $N^2 \to 0$ from the unstable stratification ψ is finite as shown by Feliks (1988). When $A_E = 0$ and when $pa \to 0$ the solution (A 12) tends to the solution of Feliks (1988) (above (A 16)) etc. The continuity of the solution into the stable regime is possible only if $A_E = 0$.

REFERENCES

Atkinson, B. W. 1981 *Meso-scale Atmospheric Circulations*. Academic.

Benjamin, T. B. 1968 Gravity currents and related phenomena. *J. Fluid Mech.* **31**, 209–248.

Crook, N. A. & Miller, M. J. 1985 A numerical and analytical study of atmospheric undular bore bore. *Qt. J. R. Met. Soc.* **111**, 225–242.

Feliks, Y. 1988 The sea-breeze front analytical model. *J. Atmos. Sci.* **45**, 1030–1038.

Haase, S. P. 1991 Numerical simulation of bore-like cold front of 8 October 1987 in Southern Germany. *Tellus* **43A**, 97–105.

Haase, S. P. & Smith, R. K. 1989*a* The numerical simulation of atmospheric gravity currents. Part I: Neutrally-stable environments. *Geophys. Astrophys. Fluid Dyn.* **46**, 1–33.

Haase, S. P. & Smith, R. K. 1989*b* The numerical simulation of atmospheric gravity currents. Part II: Environments with stable layers. *Geophys. Astrophys. Fluid Dyn.* **46**, 1–33.

Jirka, G. H. & Arita, M. 1987 Density currents or density wedges: boundary-layer influence and control methods. *J. Fluid Mech.* **177**, 187–206.

Liu, C. & Moncrieff, M. W. 1996 An analytical study of density currents in sheared, stratified fluids including the effects of latent heat. *J. Atmos. Sci.* **15**, 3303–3312.

Moncrieff, M. W. & So, D. W. K. 1989 A hydrodynamical theory of conservative bounded density currents. *J. Fluid Mech.* **198**, 177–197.

Pearson, R. A. 1973 Properties of the sea breeze front as shown by a numerical model. *J. Atmos. Sci.* **30**, 1050–1060.

Simpson, J. E., Mansfield, D. A. & Milford, J. R. 1977 Inland penetration of sea breeze fronts. *Qu. J. R. Met. Soc.* **103**, 47–76.

https://doi.org/10.1017/S0022112000001488 Published online by Cambridge University Press

Wakimoto, R. M. 1982 The life cycle thunderstorm gust fronts as viewed with Doppler radar and rawinsonde data. *Mon. Wea. Rev.* **110**, 1060–1082.

Xu, Q. 1992 Density currents in shear flows – A two-fluid model. *J. Atmos. Sci.* **49**, 511–524.

Xu, Q. & Moncrieff, M. W. 1994 Density current circulation in shear flows. *J. Atmos. Sci.* **51**, 434–446.

Xu, Q., Xue, M. & Droegemeier, K. K. 1996 Numerical simulations of density currents in sheared environment within a vertically confined channel. *J. Atmos. Sci.* **53**, 770–786.

https://doi.org/10.1017/S0022112000001488 Published online by Cambridge University Press